Lagged compound occurrence of droughts and pluvials globally over the past seven decades

Xiaogang He[1,2], **Justin Sheffield**[1,3]

[1]Department of Civil and Environmental Engineering, Princeton University, Princeton, New Jersey, USA.
[2]Water in the West, Woods Institute for the Environment, Stanford University, Stanford, California, USA.
[3]Geography and Environment, University of Southampton, Southampton, UK.

Key Points:

- We develop a novel statistical framework to quantify the spatial hotspots and temporal dynamics of the drought-pluvial seesaw.
- Globally, we find on average 11 percent of all drought events have been followed by at least one pluvial event in the following season.
- Coherent changes in seesaw frequency are not detected at the regional scale, but distinct seesaw hotspots emerge at local scales, albeit over limited land areas.

Corresponding author: Xiaogang He, Department of Civil and Environmental Engineering, Princeton, New Jersey 08544, USA, hexg@princeton.edu

This article has been accepted for publication and undergone full peer review but has not been through the copyediting, typesetting, pagination and proofreading process which may lead to differences between this version and the Version of Record. Please cite this article as doi: 10.1029/2020GL087924

Abstract

The drought-pluvial seesaw – defined as the phenomenon of pluvials (wet spells) following droughts (dry spells) – magnifies the impact of individual pluvial and drought events, yet has not been systematically evaluated, especially at the global scale. We apply an event coincidence analysis to explore the aggregated seesaw behavior based on land surface model simulations for the past seven decades (1950-2016). We find that globally, about 5.9% and 7.6% of the land surface has experienced statistically significant ($p < 0.10$) drought-pluvial seesaw behavior during the boreal spring-summer and fall-winter, with an average 11.1% and 11.4% of all droughts being followed by pluvials in the following season, respectively. Although this global frequency pattern is modest and coherent changes cannot be detected at the sub-continental scale, local hotspots of drought-pluvial seesaw have become more frequent than either droughts or pluvials alone in the last three decades, albeit with a small percentage of area coverage.

Plain Language Summary

Droughts and pluvials (also referred to as large-scale and long-term dry and wet spells) have profound impacts on a wide range of sectors, including water, agriculture and food security, energy production, infrastructure, and ecosystem health. There have been numerous studies investigating the changing behavior of droughts and pluvials and their societal impact, yet they are generally treated separately. The intersection between the two, especially the rapid transition from drought to pluvial (we call this the "drought-pluvial seesaw"), deserves more attention as it can lead to greater impact than the sum of each individual type of event because of the potential increase in vulnerability of populations and ecosystems. For example, the 2017 winter pluvials in California contributed to widespread floods, which occurred on the back of the state's multi-year (2011-2016) drought and put additional strains on the state's multiple water dependent sectors. In this study, we investigate how often droughts have been followed by pluvials in the past seven decades through a novel yet mathematically simple approach. We find that about 11 percent of droughts have been followed by at least one pluvial in the following season, although over a small percentage of the global land surface. Importantly, the swing from drought to pluvial has become more frequent in the past 30 years in some parts of the world, which may indicate greater variability in weather with climate change. Our approach could have practical value as it can inform policy-makers and local stakeholders on the often overlooked but important risk of coincident drought and pluvial, and therefore more effective water and agricultural management and adaptation plans.

1 Introduction

Weather extremes have been listed as one of the top three global risks for the past six years (2014-2019) [*World Economic Forum*, 2019], among which floods and droughts are the most common and impactful natural hazards globally. Severe floods are mainly triggered by persistent and widespread wet spells (also referred to as pluvials), either in the form of heavy precipitation events and/or through high antecedent soil moisture conditions [e.g., *Sivapalan et al.*, 2005]. Droughts are on the other end of the hydrological spectrum, usually linked to prolonged periods of low precipitation and/or dry soils. Such wet and dry events can have large impacts on agriculture and food security, water availability, energy production and natural ecosystems [e.g., *Gleick*, 1993; *Sheffield and Wood*, 2011; *He et al.*, 2019]. Globally, drought and flood losses have increased tenfold over the second half of the 20th century, to US$596 billion in the early 21st century (2000-2017) [*EM-DAT*, 2018]. A recent study [*UNISDR*, 2015] finds that, during 1995-2015, for all weather-related disasters, droughts account for 26% and affect 1.1 billion people. Pluvial events, in the form of floods, affect 2.3 billion people and account for 56% of disasters. Although a growing body of research based on climate model projections has documented that anthropogenic climate change will increase the frequency and magnitude for pluvials [e.g., *Field*, 2012; *Fischer et al.*, 2013; *Duffy et al.*, 2015; *Martin*, 2018; *Zhan et al.*, 2020] and droughts [e.g., *Sheffield and Wood*, 2008a; *Orlowsky and Seneviratne*, 2013; *Martin*, 2018], albeit with prominent regional variability, historical evidence does not show consistent changes for pluvials [e.g., *Kangas and Brown*, 2007; *Liu and Allan*, 2013; *Greve et al.*, 2014; *Lehmann et al.*, 2015, 2018] and droughts [e.g., *Sheffield and Wood*, 2008b; *Sheffield et al.*, 2012; *Dai*, 2013; *Trenberth et al.*, 2014] owing to the lack of observations, use of different metrics, as well as uncertainties from model simulations related to model structure and parameterization schemes.

Although droughts (or dry spells) and pluvials (or wet spells) are generally treated separately, there are good reasons to analyze their co-occurrence and mechanisms, and manage and mitigate their impacts concurrently for a number of reasons. Firstly, changes in frequency and intensity of droughts and pluvials are inherently interconnected and governed by the same underlying hydrological processes and atmospheric dynamics, which may lead to higher hydroclimatic variability with response to a warming climate [*Trenberth*, 1999; *Trenberth et al.*, 2003; *Giorgi et al.*, 2011]. Moreover, there are many recent examples of coincidental flood (manifested or induced by pluvial conditions) and drought events that highlight the compounded impacts of events that follow each other, and are suggestive of the expectation of a more variable climate under climate change. For instance, California recently suffered a multi-year (2011-2016) intense drought [*Diffenbaugh et al.*, 2015; *He et al.*, 2017], which caused severe environmental issues (e.g., groundwater depletion, wildfires, tree mortality) and economic losses [e.g., *Howitt et al.*, 2014]. On the heels of this prolonged drought, the state was hit by large-scale pluvial events with extreme precipitation transported from atmospheric rivers. These led to severe flooding in February 2017, which triggered a state emergency and an evacuation of 188,000 residents downstream of the Oroville Dam (California's second largest reservoir) due to its spillway failure [*NOAA National Centers for Environmental Information*, 2018]. In September 2015, there was a fast transition from drought to pluvial flooding within one week over South Carolina because of the deep tropical moisture connection to Hurricane Joaquin, which brought a once-in-a-thousand-years flood and erased the prevailing drought conditions that had lasted from May to September in 2015. This drought-pluvial seesaw also happened in the southeast U.S., where Texas experienced its worst drought in recorded history from 2010 until May 2015, which was suddenly ended by a heavy precipitation event. However, this widespread pluvial event caused flash floods, compounded the impacts of the five-year drought which has already changed the landscape and vegetation distribution significantly. The dramatic swing from severe droughts to devastating pluvials (and floods) as shown above poses a substantial risk for water management practices, especially for reservoir operation, as there exists a trade-off between short-term flood-control and long-term water-storage imperatives to satisfy water demand. In developing regions, the transition from drought to pluvial is arguably more impactful because of the compounding effects on population vulnerability. Although pluvials can sometimes alleviate drought conditions, they can have a significant effect on already impacted and more vulnerable populations if pluvials lead to severe floods [e.g., *King-Okumu et al.*, 2018].

Diagnosing the coincidence of droughts and pluvials in a changing environment [see *Lins and Slack*, 1999; *Sheffield and Wood*, 2007; *Milly et al.*, 2008; *Giorgi et al.*, 2011; *Collet et al.*, 2018] is, therefore, important for fully characterizing their impacts on water-related sectors and understanding potential adaptation strategies, such as designing more effective reservoir operation rules or agricultural planning. There is growing evidence that recent warming is leading to more extreme events in general [*Peterson et al.*, 2013] and that pluvial and drought episodes may be linked. For example, pluvial conditions are often the reason for recovery of drought conditions, such as in the southeast U.S., where tropical cyclones play a major role in drought recovery and alleviation [e.g., *Kam et al.*, 2013; *Maxwell et al.*, 2012, 2013]. In the Pacific Northwest U.S., 60-74% of persistent droughts are terminated by atmospheric rivers [*Dettinger*, 2013], and these pluvial events could help boost hydropower production. Antecedent conditions (i.e., soil moisture and snowpack conditions) can be related to changing flood risk [*Sivapalan et al.*, 2005], which can also drive drought persistence through reductions in recycled precipitation [e.g., *Dominguez et al.*, 2009]. At larger scales, pluvials and droughts are often linked because a shift in circulation drives pluvial conditions in one region while causing drought conditions in a neighboring region. For example, weakening in the East Asian summer monsoon is responsible for the spatial drought-pluvial seesaw in China, with the North and Northeast experiencing persistent and severe droughts while the Yangtze River basin in the South undergoes extreme precipitation events [*Ding et al.*, 2008]. Such seesaw oscillations have been observed spatially across the Atlantic Ocean, where pluvial flooding in the Amazon tends to coincide with Congo droughts and vice versa [*Eltahir et al.*, 2004]. Other examples include the pluvial episode in Texas and drought episode in the southeast U.S. in 2006, which were driven by a persistent shift in moisture sources from the Gulf of Mexico [*Dong et al.*, 2011]. At local scales, the transition between droughts and pluvials is related to hydrological persistence, which is controlled by land-atmosphere coupling through the complex partitioning of surface fluxes [e.g., *Ferguson and Wood*, 2011; *Roundy et al.*, 2013; *Santanello Jr et al.*, 2017]. For instance, wet/dry soils can trigger convective precipitation via positive/negative land-atmosphere feedbacks [e.g., *Eltahir and Bras*, 1996; *Taylor et al.*, 2011, 2012; *Guillod et al.*, 2015].

Nevertheless, studies focused on improving our understanding or even providing basic quantification of transitions between droughts and pluvials (also can be dubbed as "weather whiplash", *Loecke et al.* [2017]; *Swain et al.* [2018]) is lacking. The few studies that do exist are either event-based [*Seager et al.*, 2012; *Parry et al.*, 2013] or limited to regional-scales [*Dong et al.*, 2011; *Wang et al.*, 2017; *Swain et al.*, 2018] or focusing on future global warming scenarios [*Madakumbura et al.*, 2019]. A global holistic picture from the historical perspective is not available, which is due to: (1) lack of reliable datasets with long-term records, as well as a global coverage to derive robust statistical relationships; and (2) lack of novel and effective statistical models to better characterize the (lagged) coincidence between droughts and pluvials. The former can be solved via the use of large-scale hydrological modeling, which is now mature enough to provide reasonable estimates of the large-scale terrestrial water cycle. Satellite-gauge combined estimates of precipitation and other meteorological variables are available to drive these models for multiple decades that are needed to provide robust statistics [*He et al.*, 2020]. The latter can be addressed through the recent development of event-based coincidence analysis (ECA, *Donges et al.* [2016]; *Siegmund et al.* [2017]), which accounts for both the instantaneous and lagged response between climatic events, such as droughts and pluvials.

The main objective of this study is to develop a comprehensive understanding of the drought to pluvial transition (or lagged coincidence), globally over the past seven decades. This can help improve hydrological predictability and risk assessment, and therefore make disaster preparedness and risk management more effective. Given that empirical evidence, basic theory (e.g., Clausius-Clapeyron), and climate model projections suggest that pluvial and drought risk are increasing and will continue to do so in the future, we attempt to examine the inter-relationship between droughts and pluvials, including the geographical hotspots of the seesaw between them and whether this is becoming more prevalent. This is the first global study to quantify this, and not only shed light on the underlying mechanisms of the pluvial-drought cycle but also provide useful information to increase society's resilience to future swings between droughts and pluvials.

2 Materials and Methods

2.1 Drought and Pluvial Identification

We focus on large-scale and long-term drought and pluvial events (equivalent to large-scale and long-term dry and wet spells), as these events usually have larger impacts on water, agriculture, and energy sectors compared to those small scale events, and therefore deserve special attention. We consider two standardized metrics, which allow comparisons over time and space, as proxies of drought and pluvial conditions from both the meteorological and agricultural perspectives. The first one is the Standardized Precipitation Index over a one-month period (SPI1, *McKee et al.* [1993]), which is calculated using precipitation from an updated and extended version (V3) of the Princeton Global Forcings (PGF, *Sheffield et al.* [2006]; *He et al.* [2020]), from 1948 to 2016 at 0.25° spatial resolution. Calculation of SPI involves two steps. The first step is to fit a Gamma distribution to the monthly precipitation time series at each grid cell, separately for each month of the year. The second step is to transform the cumulative probability of the fitted Gamma distribution to a standard normal distribution (with mean zero and variance one). For observed precipitation at a given time scale, SPI is calculated as the number of standard deviations away from the median precipitation with negative and positive values representing precipitation deficit and surplus, respectively. We define meteorological drought at a grid cell if the monthly SPI1 is below the threshold of -1.0 [*Svoboda et al.*, 2012]. Similarly, large-scale pluvials are defined if the SPI1 exceeds 1.0. The other index is the soil moisture percentile proposed by *Sheffield et al.* [2004], which is derived from a global offline simulation of Variable Infiltration Capacity (VIC) land surface hydrological model [*Liang et al.*, 1994, 1996; *Cherkauer et al.*, 2003] forced by the PGFV3. We average the simulated daily soil moisture from the VIC model to a monthly time scale and calculate the soil moisture percentile at each grid after fitting an empirical distribution separately to each month. Previous versions of VIC simulations have been analyzed in terms of drought by *Sheffield and Wood* [2007, 2008b] and *Sheffield et al.* [2009]. The latest version of the simulation analyzed here uses updated soil parameters based on the SoilGrids1km database of soil types and profiles [*Hengl et al.*, 2014], coupled with recently developed pedotransfer functions [*Tóth et al.*, 2015] to estimate model parameters such as saturated conductivity and soil water holding capacities. These are combined with VIC-specific parameter values that were previously calibrated to river discharge measurements from a set of global river basins and evaluated against available *in situ* and remote sensing hydrological measurements, including soil moisture networks, satellite derived snow cover, water storage and evapotranspiration [*Sheffield and Wood*, 2007; *Pan et al.*, 2012]. We define an area in drought if the monthly soil moisture percentile is below a chosen threshold. The threshold value used to define a deficit is subjective as it depends on the impacted sector. As the objective is to examine drought-pluvial concurrently, it is necessary to ensure that both extremes have the same long-term occurrence rate. We therefore use the 16^{th} percentile as the threshold to identify the soil moisture drought, as this has the same cumulative probability as the SPI1-based drought threshold (SPI1<-1.0 is equivalent to the 16^{th} percentile). In a similar manner, pluvial events can be measured by the surplus soil moisture above the 84^{th} percentile.

2.2 Event Coincidence Analysis

We apply a novel yet conceptually simple method, called event coincidence analysis (ECA, *Donges et al.* [2016]; *Siegmund et al.* [2017]), to investigate the statistical interdependency between droughts and pluvials (see Figure 1). ECA can not only quantify the number of simultaneous occurrences of two extreme events (i.e., pluvials and droughts in this study), it also allows the consideration of lagged (through the time lag parameter τ) and time-uncertain (through the window size parameter ΔT) responses between them. In the case of the drought-pluvial seesaw (defined as the transition from drought to pluvial), ECA can calculate how frequently droughts are followed by pluvials with a mutual delay (τ) given a certain temporal window (ΔT) through the calculation of the so-called trigger coincidence rate $r^{\mathbf{D}\Rightarrow\mathbf{P}}$:

$$r^{\mathbf{D}\Rightarrow\mathbf{P}}(\Delta T, \tau) = \frac{1}{N_{\mathbf{D}}} \sum_{j=1}^{N_{\mathbf{D}}} \Theta\Big[\sum_{i=1}^{N_{\mathbf{P}}} \mathbf{1}_{[0,\Delta T]}((t_i^{\mathbf{P}} - \tau) - t_j^{\mathbf{D}})\Big]$$

where Θ is the Heaviside function:

$$\Theta(x) := \begin{cases} 1 & x > 0 \\ 0 & x \leq 0 \end{cases},$$

and $\mathbf{1}_{[0,\Delta T]}(\cdot)$ is the indicator function of the selected window $[0, \Delta T]$:

$$\mathbf{1}_{[0,\Delta T]}(x) := \begin{cases} 1 & \text{if } x \in [0, \Delta T] \\ 0 & \text{if } x \notin [0, \Delta T] \end{cases}.$$

$t_i^{\mathbf{P}}$ and $t_j^{\mathbf{D}}$ represent the pluvial and drought timing with total number of events $N_{\mathbf{P}}$ and $N_{\mathbf{D}}$, respectively. Here, we chose $\tau = 3$, as this represents a typical (i.e., seasonal) scale at which the large-scale hydrological conditions veer from deficit to surplus, which is critical for long-term water resources management, for example. To further quantify the robustness of the statistical interrelationship between droughts and pluvials, we conduct an analytical significance test based on the assumption of a Poisson process with the null hypothesis that the lagged coincidence between droughts and pluvials is randomly distributed (see details in Text S1). The Poisson process-based significance test is applied to each land pixel (at 0.25° spatial resolution) using monthly time series of drought and pluvial indices (see Section 2.1) extracted from that pixel. We calculate the significance level (p-value) for each pixel to assess whether the estimated seesaw occurrence rate is statistically significant or not. We also perform a comprehensive sensitivity analysis (see details in Section 4) to examine how the absolute value of the drought-pluvial seesaw frequency varies with different choices of drought/pluvial metrics (whether it is precipitation-based or soil moisture-based) and the setting of ECA (e.g., window size and time lag parameters).

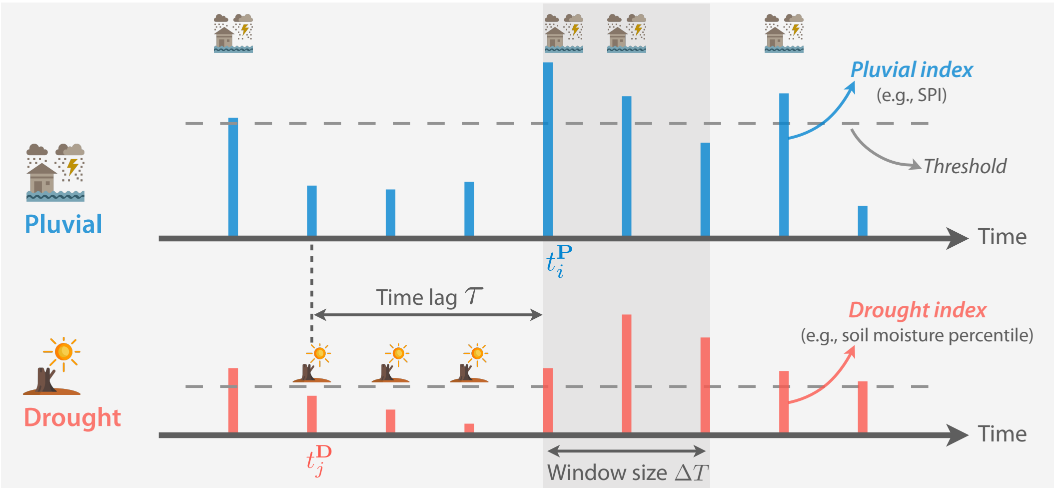

Figure 1. Schematic of the large-scale drought-pluvial seesaw based on the event coincidence analysis given the time lag (τ) between the drought occurrence timing ($t_j^{\mathbf{D}}$) and pluvial occurrence timing ($t_i^{\mathbf{P}}$) within a certain window (ΔT). Pluvial/drought events are detected when the corresponding pluvial/drought index (i.e., SPI or soil moisture percentile) exceeds/falls below the predefined threshold.

3 Results

3.1 Climatology of Drought-Pluvial Seesaw Frequency

At the global scale, we estimate an averaged seasonal drought-pluvial lagged coincidence frequency of 11.1% and 11.4% for the boreal spring-summer (April-May-June-July-August-September, AMJJAS) and boreal fall-winter (October-November-December-January-February-March, ONDJFM), respectively, during the 1950-2016 period (Figure 2, A and B). In other words, about 11% of droughts are followed by pluvials with a three-month lag after drought onset for the past seven decades. These frequencies are less than (or in specific locations, not equal to) 16%, potentially due to the effects of temporal autocorrelation. The majority (52.1% for AMJJAS and 55.6% for ONDJFM) of the global land surface (excluding Greenland, Antarctic and desert regions with annual rainfall less than 100 mm) has coincidence rates between 10% and 20%. 12.9/11.6% of the total land surface area has a coincidence rate less than 5% during AMJJAS/ONDJFM, which mainly occurred over Africa. There is a clear shift in these low frequency patterns over Southern Africa during AMJJAS and over the northern Central Africa (i.e., the transition region between deserts and tropical rainforests) during ONDJFM, which is potentially due to the seasonal movement of the Intertropical Convergence Zone (ITCZ). The climatology of seasonal drought-pluvial seesaw frequency larger than 30% is virtually non-existent (0.27/0.15% for AMJJAS/ONDJFM). Furthermore, only 5.9% (of the global land surface) of the estimated coincidence rate is locally statistically significant (with the degree of belief $\geq$ 90%) during AMJJAS, with spatially organized patterns most prominent outside of the tropics, including western territories of Canada, western coast and central part of the U.S., southeastern Brazil, northwestern Central Africa (CAF), central Democratic Republic of the Congo, the border between Kenya and Somalia, central and northeastern China, central and eastern Australia, and western Siberia (Figure 2C). There is a slight increase in the percentage of locally statistically significant area (~7.6%) during ONDJFM with robust drought-pluvial seesaw patterns over Alaska, western Canada, northwestern and central U.S., central and southern Brazil, western Russia, eastern Europe, southern Central Africa, Botswana, Iran, western and southern China (Figure 2D).

Our findings echo the observed evidence of drought-pluvial seesaw documented in previous studies. For instance, over Europe, long-term tree ring data has shown an increased volatility (i.e., more rapid shifting) between wet and dry extremes since the 1960s, which is mainly related to the increased fluctuation of the North Atlantic jet stream [*Trouet et al.*, 2018]. The seesaw hotspots detected over the Horn of Africa during AMJJAS (Figure 2C) are related to abrupt transitions in summer rainfall, which are caused by frequent summer monsoon jumps coincident with abrupt circulation changes of the Somali jet [*Riddle and Cook*, 2008]. Over the northern and southern part of the U.S. Great Plains, *Christian et al.* [2015] find that there is about 25% chance that a significant drought year is followed by a significant pluvial year, which is similar to our estimated coincidence rate, although their estimates are at annual time scale. The seasonal difference in the statistically significant clusters over Africa is likely due to the movement of the ITCZ. The scattered patterns found in the western U.S. could be related to the occurrence of atmospheric rivers, which are often associated with drought recovery [*Dettinger*, 2013], whereas over southern China, the eastern summer monsoon could contribute to the drought-pluvial seesaw [*Ding*, 1992; *Lau and Yang*, 1997; *Wu et al.*, 2006]. The robust statistical interdependency between droughts and pluvials over the southwestern and central U.S., Australia

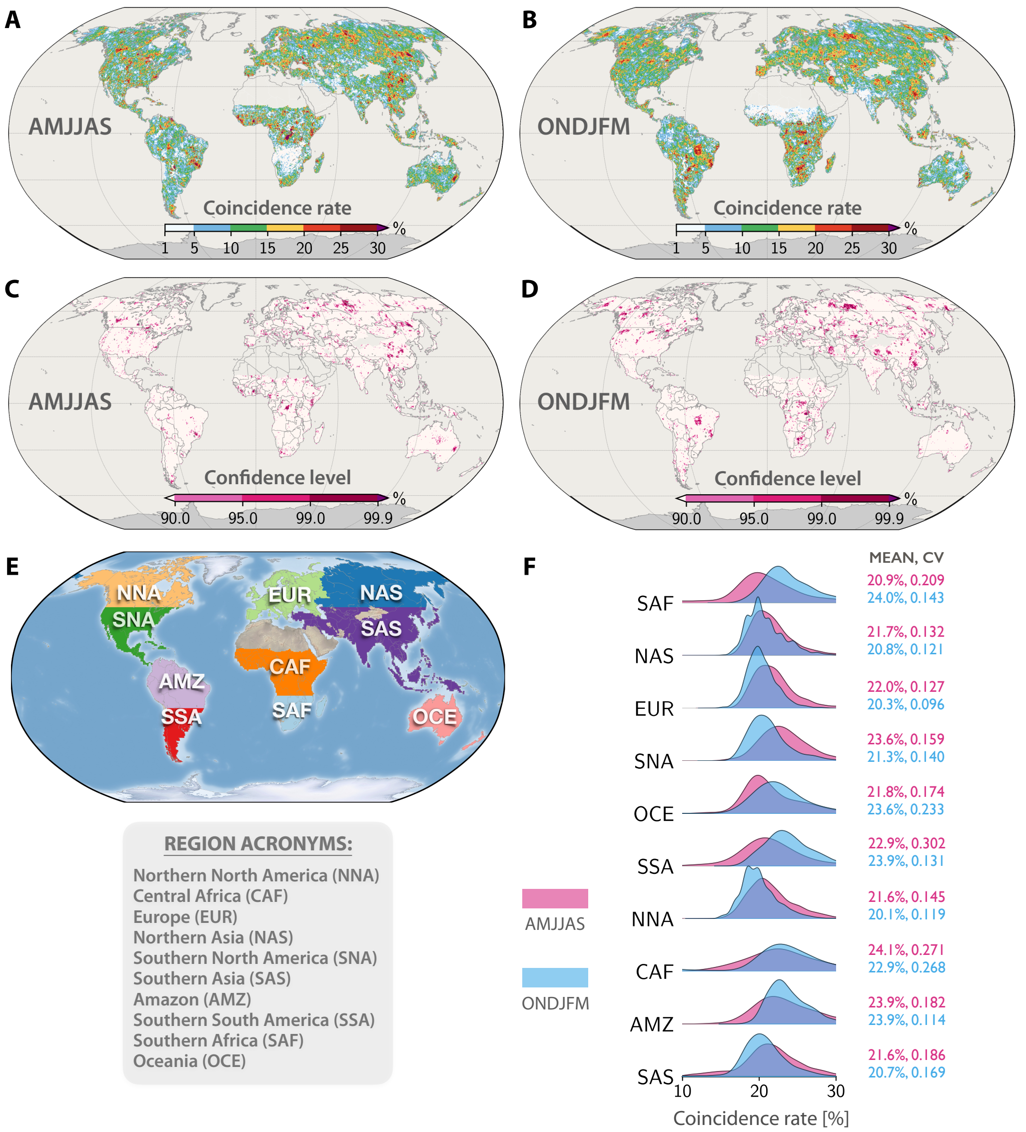

Figure 2. Frequency of drought-pluvial seesaw for the period 1950-2016. Maps show the lagged trigger coincidence rate, indicating how frequent droughts are followed by pluvials with a 3-month lag for the boreal spring-summer (AMJJAS) (A) and boreal fall-winter (ONDJFM) (B), and whether the rates are locally statistically significant based on different levels (90, 95, 99 and 99.9 percent) of significance (C and D). (E) The 10 sub-continental regions (with acronyms for brevity) used to summarize the regional statistics, covering the global land surface excluding Greenland, Antarctica and extremely dry regions with annual rainfall less than 100 mm (E). Ridgeline plots (F) showing the grid cell distributions of locally significant coincidence rates during AMJJAS and ONDJFM for each sub-region with its mean and coefficient of variation (CV).

and southern Amazon is in line with previous studies [e.g., *Fu*, 2015]. Particularly over the southern Amazon, there has been increased evidence of lengthening dryness, accompanying more frequent wet seasons [e.g., *Debortoli et al.*, 2015; *Agudelo et al.*, 2019], which result in more frequent seesaw events because of the increased intra-annual variability of the monsoon systems. Although the exact cause is still not clear, previous studies suggest that there could be multifaced mechanisms responsible for this, either due to recently intensified large-scale Walker and Hadley circulation patterns [e.g., *Badger and Dirmeyer*, 2016; *Agudelo et al.*, 2019] or because of reduced local-scale moisture recycling due to deforestation-induced land cover changes [e.g., *Fu and Li*, 2004; *Yin et al.*, 2014].

To verify the robustness of the estimated seesaw frequency at different spatially aggregated levels (e.g., country, sub-continent), we conduct field significance tests following the false discovery rate (FDR) approach [*Benjamini and Hochberg*, 1995] to account for the potential multiplicity issue [*Wilks*, 2006, 2016; *Ferguson and Mocko*, 2017]. We find that field significant see-saw frequency cannot be detected at most sub-continents, although isolated hot spots still emerge at the local scale within each region. The only exception is found over NNA, where 10% of the locally significant ($p < 0.1$) pixels are also field significant (at the $p < 0.1$ global field significant level) during ONDJFM. However, at the country level, we find that a small percentage of total pixels within the country start to pass field significance tests at $p < 0.1$ global field significant level, for instance, over the Democratic Republic of Congo, Kenya and Myanmar during AMJJAS, and over Canada, Brazil, Democratic Republic of Congo, Botswana, Iran and China during ONDJFM. These results reiterate previous findings that field significance tests can be influenced by the spatial inhomogeneities due to the geographic configuration (e.g., domain size and boundary) [*Libertino et al.*, 2019]. We further compare the differences for the two periods (Figure 2F) for the 10 sub-continent regions (Figure 2E). The spatial distribution reveals that the AMJJAS seesaw generally has higher mean values than the ONDJFM seesaw for most regions (except for SAF, OCE, and SSA), and higher spatial variability (based on the CV) except OCE. For SAF and SNA, there is a clear shift of the distribution, which is also manifested in the spatial pattern (Figure 2A and B) as the rainfall band moves, from summer to winter.

3.2 Epochal Changes in Drought, Pluvial and Seesaw Frequencies

We next calculate the frequency ratios of drought, pluvial and drought-pluvial seesaw during AMJJAS (Figure 3 and 4) and ONDJFM (Figure S1 and S2 in the supplementary information) to reflect any long-term hydrological changes. The frequency ratio is defined as the ratio of the event frequency in the last 30 years (1987-2016) to that in the first 30-year period (1950-1979). Globally, the changing frequency for droughts (Figure 3A and S1A) and pluvials (Figure 3B and S1B) is more organized and spatially coherent compared to that for drought-pluvial seesaw (Figure 3C and S1C). During AMJJAS, a prominent spatial cluster with increased drought frequency is found over southwestern and southeastern U.S., Colombia, Brazil, western Europe, majority of Africa, India, western Russia, northeast China and eastern Australia (up to five times more frequent for particular pixels). The percentage area with increased drought frequency decreases slightly during ONDJFM compared to AMJJAS, but in general, the area of increased drought frequency is still larger than that of decreased frequency for both AMJJAS and ONDJFM (Figure 3A and S1A). These spatial hotspots are consistent with previous drought exposure [*Dilley et al.*, 2005] and frequency analysis based on long-term historical records of precipitation [e.g., *Dai*, 2013; *Spinoni et al.*, 2014], Palmer Drought Severity Index (PDSI) [e.g., *Dai*, 2013] and modeled soil moisture [e.g., *Sheffield and Wood*, 2008b]. Among the 10 sub-continental regions, the probability that droughts become more frequent during AMJJAS in recent decades (Figure 4A) is evidenced for more than half of the NAS (58.4%), CAF (58.6%), and SAS (52.6%). The increased drought frequency is even more widespread over SAF (66.4%), although the percentage area decreases slightly during ONDJFM (Figure S2A). Over NAS, 10.7/11.1% of the total land surface area even exhibits frequency ratios of > 3 during AMJJAS/ONDJFM.

Different from droughts, regions experiencing increased pluvial frequency during AMJJAS in recent decades arise over a large spatial extent of central and eastern U.S., northwestern Amazon (AMZ), southern South America (SSA), Europe, Russia, and the western part of Southern Asia (SAS), especially over the Tibetan region (Figure 3B). Similar spatial patterns are found over most of these regions during ONDJFM, with increased pluvial frequency more pronounced over Europe, western Russia, the Sahel and western Australia. We also observe that for regions with increased pluvial frequency, the magnitude of frequency ratios is generally smaller than that for droughts, indicating that pluvials occur less frequently than droughts in recent decades, which is also consistent with the reduced spread of the regional distribution of pluvial frequency ratios (Figure 4B and S2B). In other words, regions with increased pluvial frequency have less spatial variability than that for droughts. Similar findings have been reported by previous global [*van der Schrier et al.*, 2013] and regional studies focusing on the U.S. [*Kangas and Brown*, 2007], Amazon

[*Marengo and Espinoza*, 2016], India [*Singh and Ranade*, 2010], and Europe [*Zolina et al.*, 2013], albeit with different observational records and metrics. Regional statistics (Figure 4B) show that recent decades have experienced an increased probability of pluvials during AMJJAS for nearly two-thirds of SNA (66.6%), more than half of NAS (52.6%), EUR (62.2%), SSA (61.1%) and NNA (59.6%). During ONDJFM, the percentage area with increased pluvial frequency increases substantially over SAF (15.7%) and OCE (48.9%) compared to AMJJAS (4.1% and 16.7%, respectively).

Compared with droughts and pluvials, we find less organized spatial structures for the increased seesaw frequency but with much higher ratios (Figure 3C and S1C), suggesting that the seasonal seesaw from droughts to pluvials has become more frequent in the recent three decades than either droughts or pluvials alone, albeit the small percentage coverage. The tendency toward more frequent seesaw is more apparent during AMJJAS (Figure 3C) than ONDJFM (Figure S1C), especially over the sub-tropics and mid-latitudes, which is also revealed from the left-skewed regional distributions (Figure 4C and S2C) with longer tails. We note an increased seesaw frequency during AMJJAS for more than half of the NAS (51.8%), ERU (50.1%), and NNA (54.0%). The elevated seesaw frequency during the recent period is particularly high with a threefold increase for more than 10% coverage of NAS, EUR and NNA for both periods. During ONDJFM, nearly one-fifth of the total data points in NNA (17.3%) exhibit ratios of > 3 (Figure S2C), which are mainly concentrated over the central U.S. (Figure S1C).

3.3 Regional Multi-Decadal Variability of Drought, Pluvial and Seesaw Frequencies

Results in the previous section only consider the two end members of the whole study period. As a complement to the spatial patterns, in this section, we quantify the temporal dynamics using a 30-year moving window (1950-1979 through 1987-2016) to capture the multi-decadal variability. We estimate regional trends based on the non-parametric, pre-whitening Mann-Kendall test [*Yue et al.*, 2002], which is robust and can effectively reduce the influence of autocorrelation. Regional trend tests for AMJJAS (Figure 5) and ONDJFM (Figure S3) suggest that overall there is little change in the seesaw frequency with a few exceptions mostly over NAS, SAS, SAF and OCE. The shading spanning the 25 and 75 percentiles of the regional event frequency indicates that seesaws have the largest spatial variability especially over tropical and Southern hemisphere regions (e.g., CAF,

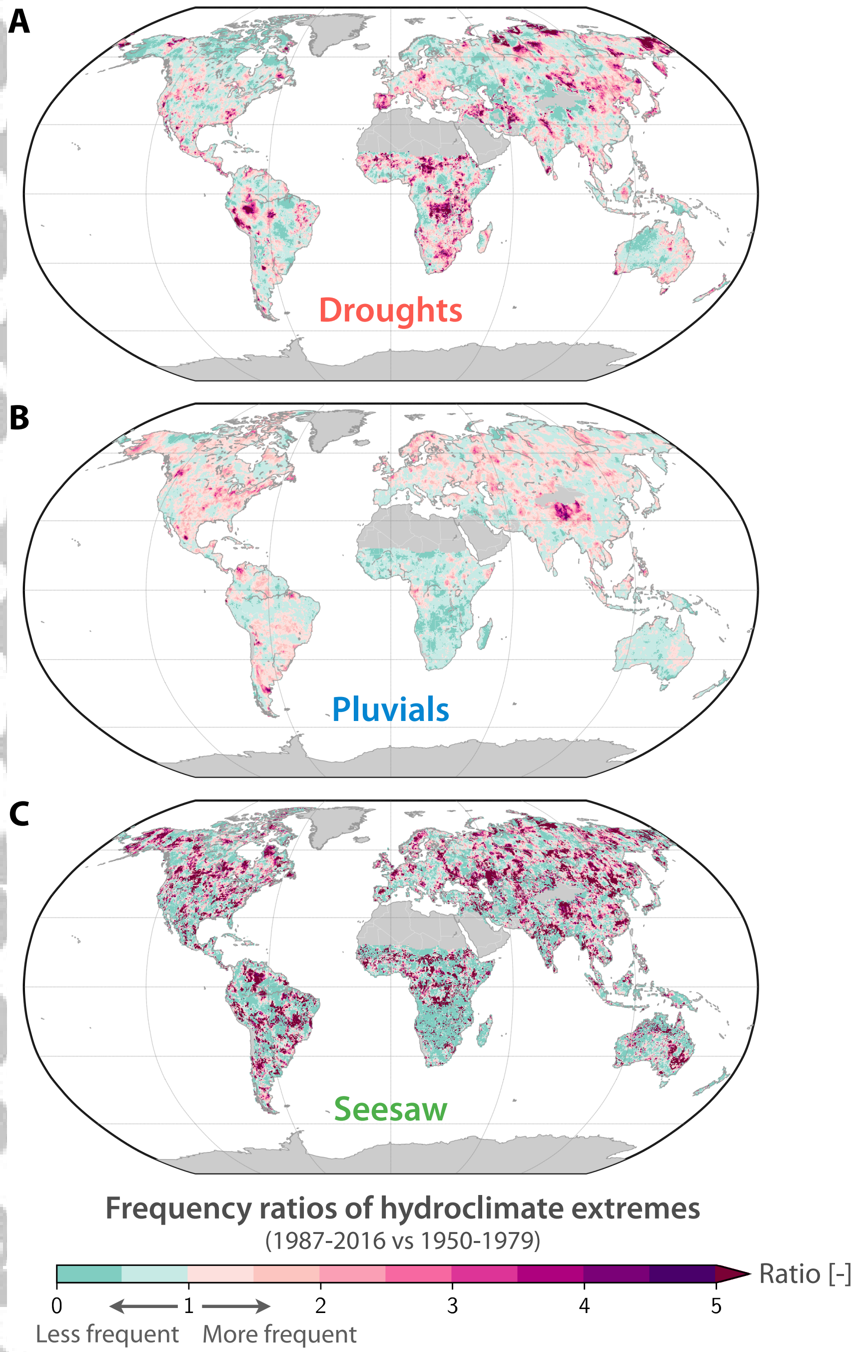

Figure 3. Maps showing relative changes of drought (A), pluvial (B) and seesaw (C) frequency in the recent 30 years (1987-2016) compared to the first 30 years (1950-1979) during AMJJAS. The relative changes are represented by frequency ratios, with values larger than 1 indicating events occurring more frequently in the recent period.

AMZ, SSA, SAF), followed by droughts, and pluvial frequency has the least spatial variability. Comparison across different regions reveals that SNA and EUR generally have the

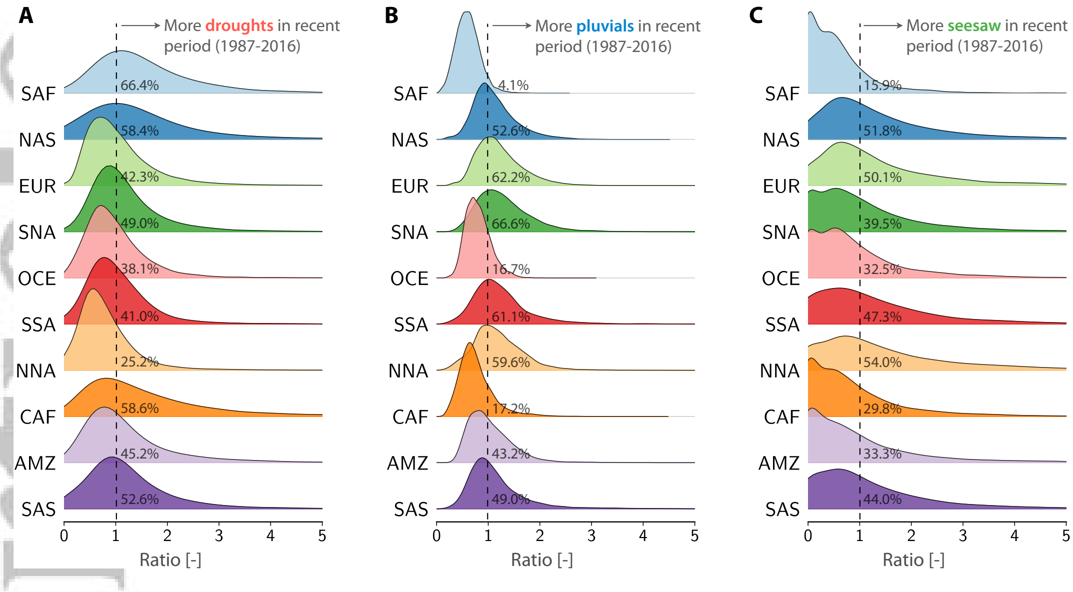

Figure 4. Ridgeline plots showing the grid cell distributions of frequency ratios for drought (A), pluvial (B), and seesaw (C) events over the 10 sub-regions.

highest seesaw frequency, whereas Africa has the lowest seesaw frequency (SAF during AMJJAS and CAF during ONDJFM). A few regions (e.g., AMZ, SSA, SAF) show an opposite trend before and after the 1970s, which might be related to the shift in the warm phase of the El Niño Southern Oscillation (ENSO) and the coincidence with increased global mean temperature [*Dai et al.*, 1998].

We find that the changing variability of the seesaw behavior is more complex than the changing variability for each individual type of event. The potential that more/less seesaw behavior will accompany increased/decreased drought and (or) pluvial frequency typically does not hold. For instance, during AMJJAS over the AMZ, even though we observe robust declining trends for both drought (-0.02% yr^{-1}, $p < 0.01$) and pluvial frequency (-0.01% yr^{-1}, $p < 0.01$), but because the magnitude is small, no robust trend is identified for the seesaw frequency (Figure 5). Similar declining trends in drought and pluvial frequencies are also found over OCE. But with a higher magnitude, this could translate to a decreasing trend of seesaw occurrence. In contrast, albeit that no robust trends are found for either droughts or pluvials over SAS during AMJJAS and SNA during ONDJFM, increasing trends of seesaw frequency are detected for both regions, although with different degrees of significance ($p < 0.01$ for SAS and $p < 0.1$ for SNA). In another case, only one end of the hydroclimate spectrum (i.e., either pluvial or drought, but not both) experiences a robust trend, but the trend in seesaw is still statistically significant. This happens over SSA during AMJJAS, where robust increasing trends are only detected for pluvials (0.06% yr^{-1}, $p < 0.1$) and seesaw (0.04% yr^{-1}, $p < 0.05$). A similar trait is shared by SAF during AMJJAS, but with robust declining trends for both events. This also happens in Asia (NAS and SAS) during ONDJFM, where a robust trend of seesaw frequency is accompanied by a robust trend of pluvial frequency, but is essentially zero over NAS for both pluvial (-0.001% yr^{-1}, $p < 0.05$) and seesaw (-0.003% yr^{-1}, $p < 0.05$). In contrast, the robust and substantial changing trends of seesaw frequency over AMZ (-0.10% yr^{-1}, $p < 0.01$) and OCE (0.13% yr^{-1}, $p < 0.01$) during ONDJFM are concomitant with the robust trend of drought frequency. Only few regions experience robust trends for all three types of events. This includes NAS and OCE during AMJJAS, with the former having more pronounced increases in drought occurrence (0.11% yr^{-1}, $p < 0.01$), whereas the latter has more pronounced decreases in pluvial occurrence (-0.08% yr^{-1}, $p < 0.01$) compared to the other two events. During ONDJFM, we observe a positive trend of seesaw occurrence (0.06% yr^{-1}, $p < 0.01$) over EUR, which coincides with the negative trend of drought occurrence (-0.11% yr^{-1}, $p < 0.01$) and positive trend of pluvial occurrence (0.08% yr^{-1}, $p < 0.01$). There has been a decreasing trend of the seesaw from droughts to pluvials over SAF (-0.04% yr^{-1}, $p < 0.05$), mainly due to the negative trend of pluvial occurrence (-0.12% yr^{-1}, $p < 0.01$), albeit with increased occurrence of droughts towards the more recent period (0.03% yr^{-1}, $p < 0.01$).

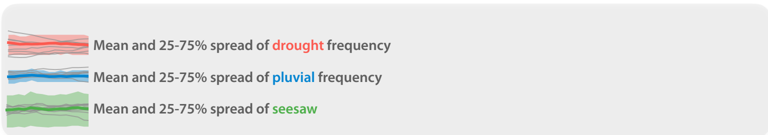

Figure 5. Temporal dynamics of the drought (top panel), pluvial (middle panel) and seesaw (bottom panel) frequencies calculated from a 30-year moving window with thick lines showing the areal means and shaded areas spanning the 25^{th} and 75^{th} percentiles of grid cell values for each region for drought (orange), pluvial (blue) and seesaw (green). Each panel has a cluster of 10 grey lines, which show the ensemble of the regional averaged frequencies for the 10 sub-continents. Upward/Downward arrow in each panel indicates that there is a statistically significant increasing/decreasing trend based on different levels of significance (represented by different numbers of stars).

4 Discussion and Conclusions

Droughts and pluvials have been widely studied, yet their interrelationship (the transition from one type to the other) has not been systematically examined, especially at the global scale from the historical perspective. Using event coincidence analysis we find that globally, about 5.9% and 7.6% of the land surface has experienced statistically significant ($p < 0.10$) drought-pluvial seesaw during the boreal spring-summer (AMJJAS) and fall-winter (ONDJFM), with an averaged 11.1% and 11.4% of all droughts being followed by pluvials in the next season, respectively. Although the overall percentage area of seesaw occurrence is small, we identify regional hotspots, mainly in the mid-latitude regions, which have experienced an increase in the frequency of droughts, pluvials and drought-pluvial seesaw in the historical period.

It should be noted that the estimated probability of lagged concurrent droughts and pluvials depends on the settings of the proposed framework, including the definition of drought and pluvial events related to the threshold (e.g., high vs low) and choice of metrics (e.g., whether they are precipitation-based or soil moisture-based), the pre-defined time lag (which determines the rapidness of event transition) and the selected temporal window size (which characterizes the uncertain timing of event occurrence). Researchers should therefore tailor the proposed framework to a specific sector and impact related setting. From the disaster management point of view, the time lag parameter τ indicates how fast societies can respond to and prepare for the rapid transition from droughts to pluvials, whereas the coincidence interval ΔT can be related to models' forecast skill, for instance, the uncertain onset of extreme events. Sensitivity analysis (Figure S4, S5, S6) reveals that regional averaged drought-pluvial coincidence rate is more sensitive to the uncertainty of event timing (as represented by ΔT) compared to the delay between events (as represented by τ). This highlights the importance of reducing uncertainties in the predicted onset of extremes, which is still challenging especially at seasonal and even longer timescales [*Hao et al.*, 2018]. In fact, the increased coincidence rates with larger window size is not surprising, as a larger window tends to cover more events, which inevitably increases the lagged concurrency of droughts and pluvials. Using precipitation-based indices for both droughts and pluvials identification (Figure S5) yields similar results compared to the combination of soil moisture-based droughts and precipitation-based pluvials (Figure S4). However, there is a significant decrease in the magnitude of regional coincidence rate but amplified regional differences, if droughts and pluvials are both identified using soil moisture percentile (Figure S6). These sensitivity results highlight the complicated dynamics that can introduce a disconnect between precipitation-based and land surface water-based representations of dryness and wetness via the propagation through the hydrological cycle.

Explaining these patterns from a physical standpoint is difficult, given that the mechanisms for individual types of events are complex, let alone the intertwined relationship between the two. An understanding of the drought-pluvial seesaw is therefore difficult to identify, especially at the global scale; the transition from drought to pluvial is likely case dependent, and influenced not only by climate variability but potentially also by climate change, and therefore difficult to disentangle. Nevertheless, a critical question is whether the identified historic changes in drought-pluvial seesaw frequency in the regional hotspots are due to climate change and therefore a sign of potential further changes in the future. Numerous studies have demonstrated that with a warming climate, drought risk/frequency could be elevated due to increased evapotranspiration induced by increased temperature [e.g., *Sheffield and Wood*, 2008a; *Zhan et al.*, 2020]. At the same time, the probability of extreme rainfall events is expected to increase, as the atmosphere can hold more moisture from the increased evapotranspiration, which can contribute to increased pluvial risk [e.g., *Zhan et al.*, 2020]. On top of these overall trends, warming-induced changes in global climate variability, such as El Niño/La Niña [e.g., *Yu et al.*, 2017; *Fasullo et al.*, 2018], or Artic sea ice [e.g., *Francis et al.*, 2017; *Coumou et al.*, 2018] can bring more year-to-year variability or persistence in weather patterns, substantially influencing regional precipitation and temperature anomalies. Direct human interventions could further exacerbate drought risk (due to increased human water consumption through irrigation and groundwater pumping, *Wada et al.* [2013]; *He et al.* [2017]) and pluvial-induced flood risk (due to land use changes including urbanization [e.g., *Yang et al.*, 2013] and agricultural practices [e.g., *Villarini and Strong*, 2014], as well as levee and dam construction as demonstrated by *Munoz et al.* [2018] at the local scale). Therefore, it remains to be seen to what extent future seesaw frequency will respond to anthropogenic forcing, internal atmospheric processes as well as human interventions.

Droughts, pluvials and their rapid transitions are inevitable, but fatalities, infrastructure failure and economic losses are not. The regional hotspots we identified, such as in Africa, generally have high vulnerability to pluvials and droughts, which can be exacerbated when there is a rapid transition between events, with an already impacted population being even more vulnerable to a subsequent hazard. The framework developed in this study could therefore be of practical value to inform policy-makers and local stakeholders on the potential risks and therefore more effective water and agricultural management policies and robust mitigation plans.

Acknowledgements

This material was based upon work supported by NOAA grant NA14OAR4310218 and the Princeton Environmental Institute at Princeton University through the Mary and Randall Hack '69 Research Fund. The latest Princeton Global Forcing (PGF) datasets, VIC land surface model simulations and derived drought indices are available at: `http://hydrology.princeton.edu/data/hexg/GDFC/`. Details can be found in *He et al.* [2020].

References

Agudelo, J., P. A. Arias, S. C. Vieira, and J. A. Martínez (2019), Influence of longer dry seasons in the Southern Amazon on patterns of water vapor transport over northern South America and the Caribbean, *Climate Dynamics*, *52*, 2647–2665.

Badger, A. M., and P. A. Dirmeyer (2016), Remote tropical and sub-tropical responses to Amazon deforestation, *Climate Dynamics*, *46*, 3057–3066.

Benjamini, Y., and Y. Hochberg (1995), Controlling the false discovery rate: A practical and powerful approach to multiple testing, *Journal of the royal statistical society. Series B (Methodological)*, pp. 289–300.

Cherkauer, K. A., L. C. Bowling, and D. P. Lettenmaier (2003), Variable infiltration capacity cold land process model updates, *Global and Planetary Change*, *38*(1-2), 151–159.

Christian, J., K. Christian, and J. B. Basara (2015), Drought and pluvial dipole events within the great plains of the United States, *Journal of Applied Meteorology and Climatology*, *54*(9), 1886–1898.

Collet, L., S. Harrigan, C. Prudhomme, G. Formetta, and L. Beevers (2018), Future hotspots for hydro-hazards in Great Britain: A probabilistic assessment, *Hydrology and Earth System Sciences*, *22*(10), 5387–5401.

Coumou, D., G. Di Capua, S. Vavrus, L. Wang, and S. Wang (2018), The influence of Arctic amplification on mid-latitude summer circulation, *Nature communications*, *9*(1), 2959.

Dai, A. (2013), Increasing drought under global warming in observations and models, *Nature Climate Change*, *3*(1), 52–58.

Dai, A., K. E. Trenberth, and T. R. Karl (1998), Global variations in droughts and wet spells: 1900–1995, *Geophysical Research Letters*, *25*(17), 3367–3370.

Debortoli, N. S., V. Dubreuil, B. Funatsu, F. Delahaye, C. H. De Oliveira, S. Rodrigues-Filho, C. H. Saito, and R. Fetter (2015), Rainfall patterns in the Southern Amazon: A chronological perspective (1971–2010), *Climatic Change*, *132*(2), 251–264.

Dettinger, M. D. (2013), Atmospheric rivers as drought busters on the US West Coast, *Journal of Hydrometeorology*, *14*(6), 1721–1732.

Diffenbaugh, N. S., D. L. Swain, and D. Touma (2015), Anthropogenic warming has increased drought risk in California, *Proceedings of the National Academy of Sciences*, *112*(13), 3931–3936.

Dilley, M., R. S. Chen, U. Deichmann, A. L. Lerner-Lam, and M. Arnold (2005), *Natural disaster hotspots: A global risk analysis*, The World Bank.

Ding, Y. (1992), Summer monsoon rainfalls in China, *Journal of the Meteorological Society of Japan. Ser. II*, *70*(1B), 373–396.

Ding, Y., Z. Wang, and Y. Sun (2008), Inter-decadal variation of the summer precipitation in East China and its association with decreasing Asian summer monsoon. Part I: Observed evidences, *International Journal of Climatology*, *28*(9), 1139–1161.

Dominguez, F., J. C. Villegas, and D. D. Breshears (2009), Spatial extent of the North American Monsoon: Increased cross-regional linkages via atmospheric pathways, *Geophysical Research Letters*, *36*(7).

Dong, X., B. Xi, A. Kennedy, Z. Feng, J. K. Entin, P. R. Houser, R. A. Schiffer, T. L'Ecuyer, W. S. Olson, K.-l. Hsu, et al. (2011), Investigation of the 2006 drought and 2007 flood extremes at the Southern Great Plains through an integrative analysis of observations, *Journal of Geophysical Research: Atmospheres*, *116*(D3).

Donges, J., C.-F. Schleussner, J. Siegmund, and R. Donner (2016), Event coincidence analysis for quantifying statistical interrelationships between event time series, *The European Physical Journal Special Topics*, *225*(3), 471–487.

Duffy, P. B., P. Brando, G. P. Asner, and C. B. Field (2015), Projections of future meteorological drought and wet periods in the Amazon, *Proceedings of the National Academy of Sciences*, *112*(43), 13,172–13,177.

Eltahir, E. A., and R. L. Bras (1996), Precipitation recycling, *Reviews of Geophysics*, *34*(3), 367–378.

Eltahir, E. A., B. Loux, T. K. Yamana, and A. Bomblies (2004), A see-saw oscillation between the Amazon and Congo basins, *Geophysical Research Letters*, *31*(23).

EM-DAT (2018), The International Disaster Database, https://www.emdat.be/, accessed: 2018-10-20.

Fasullo, J., B. Otto-Bliesner, and S. Stevenson (2018), ENSO's changing influence on temperature, precipitation, and wildfire in a warming climate, *Geophysical Research Letters*, *45*, 9216–9225.

Ferguson, C. R., and D. M. Mocko (2017), Diagnosing an artificial trend in NLDAS-2 afternoon precipitation, *Journal of Hydrometeorology*, *18*(4), 1051–1070.

Ferguson, C. R., and E. F. Wood (2011), Observed land–atmosphere coupling from satellite remote sensing and reanalysis, *Journal of Hydrometeorology*, *12*(6), 1221–1254.

Field, C. B. (2012), *Managing the risks of extreme events and disasters to advance climate change adaptation: Special report of the intergovernmental panel on climate change*, Cambridge University Press.

Fischer, E. M., U. Beyerle, and R. Knutti (2013), Robust spatially aggregated projections of climate extremes, *Nature Climate Change*, *3*(12), 1033–1038.

Francis, J. A., S. J. Vavrus, and J. Cohen (2017), Amplified Arctic warming and mid-latitude weather: New perspectives on emerging connections, *Wiley Interdisciplinary Reviews: Climate Change*, *8*(5), e474.

Fu, R. (2015), Global warming-accelerated drying in the tropics, *Proceedings of the National Academy of Sciences*, *112*(12), 3593–3594.

Fu, R., and W. Li (2004), The influence of the land surface on the transition from dry to wet season in Amazonia, *Theoretical and Applied Climatology*, *78*(1-3), 97–110.

Giorgi, F., E.-S. Im, E. Coppola, N. Diffenbaugh, X. Gao, L. Mariotti, and Y. Shi (2011), Higher hydroclimatic intensity with global warming, *Journal of Climate*, *24*(20), 5309–5324.

Gleick, P. H. (1993), *Water in crisis: A guide to the worlds fresh water resources*, Oxford University Press, New York.

Greve, P., B. Orlowsky, B. Mueller, J. Sheffield, M. Reichstein, and S. I. Seneviratne (2014), Global assessment of trends in wetting and drying over land, *Nature Geoscience*, *7*(10), 716–721.

Guillod, B. P., B. Orlowsky, D. G. Miralles, A. J. Teuling, and S. I. Seneviratne (2015), Reconciling spatial and temporal soil moisture effects on afternoon rainfall, *Nature communications*, *6*, 6443.

Hao, Z., V. P. Singh, and Y. Xia (2018), Seasonal drought prediction: Advances, challenges, and future prospects, *Reviews of Geophysics*, *56*(1), 108–141.

He, X., Y. Wada, N. Wanders, and J. Sheffield (2017), Intensification of hydrological drought in California by human water management, *Geophysical Research Letters*, *44*(4), 1777–1785, doi:10.1002/2016GL071665.

He, X., L. Estes, M. Konar, D. Tian, D. Anghileri, K. Baylis, T. P. Evans, and J. Sheffield (2019), Integrated approaches to understanding and reducing drought impact on food security across scales, *Current Opinion in Environmental Sustainability*, *40*, 43–54.

He, X., M. Pan, Z. Wei, E. F. Wood, and J. Sheffield (2020), A global drought and flood catalogue from 1950 to 2016, *Bulletin of the American Meteorological Society*, doi:10.1175/BAMS-D-18-0269.1.

Hengl, T., J. M. de Jesus, R. A. MacMillan, N. H. Batjes, G. B. Heuvelink, E. Ribeiro, A. Samuel-Rosa, B. Kempen, J. G. Leenaars, M. G. Walsh, et al. (2014), SoilGrids1km – global soil information based on automated mapping, *PLoS One*, *9*(8), e105,992.

Howitt, R., J. Medellín-Azuara, D. MacEwan, J. Lund, and D. Sumner (2014), Economic analysis of the 2014 drought for California agriculture, *Center for Watershed Sciences, University of California, Davis*.

Kam, J., J. Sheffield, X. Yuan, and E. F. Wood (2013), The influence of Atlantic tropical cyclones on drought over the eastern United States (1980–2007), *Journal of Climate*, *26*(10), 3067–3086.

Kangas, R. S., and T. J. Brown (2007), Characteristics of US drought and pluvials from a high-resolution spatial dataset, *International Journal of Climatology: A Journal of the Royal Meteorological Society*, *27*(10), 1303–1325.

King-Okumu, C., B. Jillo, J. Kinyanjui, and I. Jarso (2018), Devolving water governance in the Kenyan Arid Lands: From top-down drought and flood emergency response to locally driven water resource development planning, *International Journal of Water Resources Development*, *34*(4), 675–697.

Lau, K., and S. Yang (1997), Climatology and interannual variability of the Southeast Asian summer monsoon, *Advances in Atmospheric Sciences*, *14*(2), 141–162.

Lehmann, J., D. Coumou, and K. Frieler (2015), Increased record-breaking precipitation events under global warming, *Climatic Change*, *132*(4), 501–515.

Lehmann, J., F. Mempel, and D. Coumou (2018), Increased occurrence of record-wet and record-dry months reflect changes in mean rainfall, *Geophysical Research Letters*, *45*, doi:10.1029/2018GL079439.

Liang, X., D. P. Lettenmaier, E. F. Wood, and S. J. Burges (1994), A simple hydrologically based model of land surface water and energy fluxes for general circulation models, *Journal of Geophysical Research: Atmospheres*, *99*(D7), 14,415–14,428.

Liang, X., E. F. Wood, and D. P. Lettenmaier (1996), Surface soil moisture parameterization of the VIC-2L model: Evaluation and modification, *Global and Planetary Change*, *13*(1-4), 195–206.

Libertino, A., D. Ganora, and P. Claps (2019), Evidence for increasing rainfall extremes remains elusive at large spatial scales: The case of Italy, *Geophysical Research Letters*, *46*, 1–10.

Lins, H. F., and J. R. Slack (1999), Streamflow trends in the United States, *Geophysical research letters*, *26*(2), 227–230.

Liu, C., and R. P. Allan (2013), Observed and simulated precipitation responses in wet and dry regions 1850–2100, *Environmental Research Letters*, *8*(3), 034,002.

Loecke, T. D., A. J. Burgin, D. A. Riveros-Iregui, A. S. Ward, S. A. Thomas, C. A. Davis, and M. A. S. Clair (2017), Weather whiplash in agricultural regions drives deterioration of water quality, *Biogeochemistry*, *133*(1), 7–15.

Madakumbura, G. D., H. Kim, N. Utsumi, H. Shiogama, E. M. Fischer, Ø. Seland, J. F. Scinocca, D. M. Mitchell, Y. Hirabayashi, and T. Oki (2019), Event-to-event intensification of the hydrologic cycle from 1.5 °C to a 2 °C warmer world, *Scientific Reports*, *9*(1), 3483.

Marengo, J. A., and J. Espinoza (2016), Extreme seasonal droughts and floods in Amazonia: Causes, trends and impacts, *International Journal of Climatology*, *36*(3), 1033–1050.

Martin, E. (2018), Future projections of global pluvial and drought event characteristics, *Geophysical Research Letters*, *45*(21), 11–913.

Maxwell, J. T., P. T. Soulé, J. T. Ortegren, and P. A. Knapp (2012), Drought-busting tropical cyclones in the southeastern Atlantic United States: 1950–2008, *Annals of the Association of American Geographers*, *102*(2), 259–275.

Maxwell, J. T., J. T. Ortegren, P. A. Knapp, and P. T. Soulé (2013), Tropical cyclones and drought amelioration in the Gulf and southeastern coastal United States, *Journal of Climate*, *26*(21), 8440–8452.

McKee, T. B., N. J. Doesken, J. Kleist, et al. (1993), The relationship of drought frequency and duration to time scales, in *Proceedings of the 8th Conference on Applied Climatology*, vol. 17, pp. 179–183, American Meteorological Society Boston, MA.

Milly, P., J. Betancourt, M. Falkenmark, R. M. Hirsch, Z. W. Kundzewicz, D. P. Lettenmaier, and R. J. Stouffer (2008), Stationarity is dead: Whither water management?, *Science*, *319*(5863), 573–574.

Munoz, S. E., L. Giosan, M. D. Therrell, J. W. Remo, Z. Shen, R. M. Sullivan, C. Wiman, M. O'Donnell, and J. P. Donnelly (2018), Climatic control of Mississippi

River flood hazard amplified by river engineering, *Nature*, *556*(7699), 95–98.

NOAA National Centers for Environmental Information (2018), U.S. Billion-Dollar Weather and Climate Disasters (2018), https://www.ncdc.noaa.gov/billions/, accessed: 2018-08-20.

Orlowsky, B., and S. I. Seneviratne (2013), Elusive drought: Uncertainty in observed trends and short-and long-term CMIP5 projections, *Hydrology and Earth System Sciences*, *17*(5), 1765–1781.

Pan, M., A. K. Sahoo, T. J. Troy, R. K. Vinukollu, J. Sheffield, and E. F. Wood (2012), Multisource estimation of long-term terrestrial water budget for major global river basins, *Journal of Climate*, *25*(9), 3191–3206.

Parry, S., T. Marsh, and M. Kendon (2013), 2012: From drought to floods in England and Wales, *Weather*, *68*(10), 268–274.

Peterson, T. C., M. P. Hoerling, P. A. Stott, and S. C. Herring (2013), Explaining extreme events of 2012 from a climate perspective, *Bulletin of the American Meteorological Society*, *94*(9), S1–S74.

Riddle, E. E., and K. H. Cook (2008), Abrupt rainfall transitions over the Greater Horn of Africa: Observations and regional model simulations, *Journal of Geophysical Research: Atmospheres*, *113*(D15).

Roundy, J. K., C. R. Ferguson, and E. F. Wood (2013), Temporal variability of land–atmosphere coupling and its implications for drought over the southeast United States, *Journal of Hydrometeorology*, *14*(2), 622–635.

Santanello Jr, J. A., P. A. Dirmeyer, C. R. Ferguson, K. L. Findell, A. B. Tawfik, A. Berg, M. Ek, P. Gentine, B. P. Guillod, C. van Heerwaarden, et al. (2017), Land-atmosphere interactions: The LoCo perspective, *Bulletin of the American Meteorological Society*, pp. 1253–1272.

Seager, R., N. Pederson, Y. Kushnir, J. Nakamura, and S. Jurburg (2012), The 1960s drought and the subsequent shift to a wetter climate in the Catskill Mountains region of the New York City watershed, *Journal of Climate*, *25*(19), 6721–6742.

Sheffield, J., and E. F. Wood (2007), Characteristics of global and regional drought, 1950–2000: Analysis of soil moisture data from off-line simulation of the terrestrial hydrologic cycle, *Journal of Geophysical Research: Atmospheres*, *112*(D17).

Sheffield, J., and E. F. Wood (2008a), Projected changes in drought occurrence under future global warming from multi-model, multi-scenario, IPCC AR4 simulations, *Climate*

Dynamics, *31*(1), 79–105.

Sheffield, J., and E. F. Wood (2008b), Global trends and variability in soil moisture and drought characteristics, 1950–2000, from observation-driven simulations of the terrestrial hydrologic cycle, *Journal of Climate*, *21*(3), 432–458.

Sheffield, J., and E. F. Wood (2011), *Drought: Past problems and future scenarios*, Earthscan, London.

Sheffield, J., G. Goteti, F. Wen, and E. F. Wood (2004), A simulated soil moisture based drought analysis for the United States, *Journal of Geophysical Research: Atmospheres*, *109*(D24).

Sheffield, J., G. Goteti, and E. F. Wood (2006), Development of a 50-year high-resolution global dataset of meteorological forcings for land surface modeling, *Journal of Climate*, *19*(13), 3088–3111.

Sheffield, J., K. Andreadis, E. F. Wood, and D. P. Lettenmaier (2009), Global and continental drought in the second half of the twentieth century: Severity-area-duration analysis and temporal variability of large-scale events, *Journal of Climate*, *22*(8), 1962–1981.

Sheffield, J., E. F. Wood, and M. L. Roderick (2012), Little change in global drought over the past 60 years, *Nature*, *491*(7424), 435–438.

Siegmund, J. F., N. Siegmund, and R. V. Donner (2017), CoinCalc – A new R package for quantifying simultaneities of event series, *Computers & Geosciences*, *98*, 64–72.

Singh, N., and A. Ranade (2010), The wet and dry spells across India during 1951–2007, *Journal of Hydrometeorology*, *11*(1), 26–45.

Sivapalan, M., G. Blöschl, R. Merz, and D. Gutknecht (2005), Linking flood frequency to long-term water balance: Incorporating effects of seasonality, *Water Resources Research*, *41*(6).

Spinoni, J., G. Naumann, H. Carrao, P. Barbosa, and J. Vogt (2014), World drought frequency, duration, and severity for 1951–2010, *International Journal of Climatology*, *34*(8), 2792–2804.

Svoboda, M., M. Hayes, and D. Wood (2012), Standardized precipitation index user guide, *World Meteorological Organization Geneva, Switzerland.*

Swain, D. L., B. Langenbrunner, J. D. Neelin, and A. Hall (2018), Increasing precipitation volatility in twenty-first-century California, *Nature Climate Change*, *8*(5), 427–433.

Taylor, C. M., A. Gounou, F. Guichard, P. P. Harris, R. J. Ellis, F. Couvreux, and M. De Kauwe (2011), Frequency of Sahelian storm initiation enhanced over mesoscale soil-moisture patterns, *Nature Geoscience*, *4*(7), 430–433.

Taylor, C. M., R. A. de Jeu, F. Guichard, P. P. Harris, and W. A. Dorigo (2012), Afternoon rain more likely over drier soils, *Nature*, *489*(7416), 423–426.

Tóth, B., M. Weynants, A. Nemes, A. Makó, G. Bilas, and G. Tóth (2015), New generation of hydraulic pedotransfer functions for Europe, *European journal of soil science*, *66*(1), 226–238.

Trenberth, K. E. (1999), Conceptual framework for changes of extremes of the hydrological cycle with climate change, in *Weather and Climate Extremes*, pp. 327–339, Springer.

Trenberth, K. E., A. Dai, R. M. Rasmussen, and D. B. Parsons (2003), The changing character of precipitation, *Bulletin of the American Meteorological Society*, *84*(9), 1205–1218.

Trenberth, K. E., A. Dai, G. van der Schrier, P. D. Jones, J. Barichivich, K. R. Briffa, and J. Sheffield (2014), Global warming and changes in drought, *Nature Climate Change*, *4*(1), 17–22.

Trouet, V., F. Babst, and M. Meko (2018), Recent enhanced high-summer North Atlantic Jet variability emerges from three-century context, *Nature communications*, *9*(180).

UNISDR (2015), *The human cost of weather related disasters*, The UN Office for Disaster Risk Reduction.

van der Schrier, G., J. Barichivich, K. Briffa, and P. Jones (2013), A scPDSI-based global data set of dry and wet spells for 1901–2009, *Journal of Geophysical Research: Atmospheres*, *118*(10), 4025–4048.

Villarini, G., and A. Strong (2014), Roles of climate and agricultural practices in discharge changes in an agricultural watershed in Iowa, *Agriculture, ecosystems & environment*, *188*, 204–211.

Wada, Y., L. P. H. van Beek, N. Wanders, and M. F. P. Bierkens (2013), Human water consumption intensifies hydrological drought worldwide, *Environmental Research Letters*, *8*(3), 034–036.

Wang, S.-Y. S., J.-H. Yoon, E. Becker, and R. Gillies (2017), California from drought to deluge, *Nature Climate Change*, *7*(7), 465–468.

Wilks, D. (2006), On “field significance" and the false discovery rate, *Journal of Applied Meteorology and Climatology*, *45*(9), 1181–1189.

Wilks, D. S. (2016), “the stippling shows statistically significant grid points”: How research results are routinely overstated and overinterpreted, and what to do about it, *Bul-*

letin of the American Meteorological Society, *97*(12), 2263–2273.

World Economic Forum (2019), The global risks report 2019.

Wu, Z., J. Li, J. He, and Z. Jiang (2006), Occurrence of droughts and floods during the normal summer monsoons in the mid-and lower reaches of the Yangtze River, *Geophysical Research Letters*, *33*(5).

Yang, L., J. A. Smith, D. B. Wright, M. L. Baeck, G. Villarini, F. Tian, and H. Hu (2013), Urbanization and climate change: An examination of nonstationarities in urban flooding, *Journal of Hydrometeorology*, *14*(6), 1791–1809.

Yin, L., R. Fu, Y.-F. Zhang, P. A. Arias, D. N. Fernando, W. Li, K. Fernandes, and A. R. Bowerman (2014), What controls the interannual variation of the wet season onsets over the Amazon?, *Journal of Geophysical Research: Atmospheres*, *119*(5), 2314–2328.

Yu, J.-Y., X. Wang, S. Yang, H. Paek, and M. Chen (2017), The changing El Niño–Southern Oscillation and associated climate extremes, *Climate Extremes: Patterns and Mechanisms*, pp. 1–38.

Yue, S., P. Pilon, B. Phinney, and G. Cavadias (2002), The influence of autocorrelation on the ability to detect trend in hydrological series, *Hydrological Processes*, *16*(9), 1807–1829.

Zhan, W., X. He, J. Sheffield, and E. F. Wood (2020), Projected seasonal changes in large-scale global precipitation and temperature extremes based on the CMIP5 ensemble, *Journal of Climate*.

Zolina, O., C. Simmer, K. Belyaev, S. K. Gulev, and P. Koltermann (2013), Changes in the duration of European wet and dry spells during the last 60 years, *Journal of Climate*, *26*(6), 2022–2047.